Single spin resonance driven by electric modulation of the *g*-factor anisotropy

A. Ferrón [1,*], S. A. Rodríguez,[1] S. S. Gómez,[1] J. L. Lado,[2] and J. Fernández-Rossier[3,†]

[1]*Instituto de Modelado e Innovación Tecnológica (CONICET-UNNE) and Facultad de Ciencias Exactas, Naturales y Agrimensura, Universidad Nacional del Nordeste, Avenida Libertad 5400, W3404AAS Corrientes, Argentina*
[2]*Department of Applied Physics, Aalto University, Espoo, Finland*
[3]*QuantaLab, International Iberian Nanotechnology Laboratory (INL), Avenida Mestre José Veiga, 4715-330 Braga, Portugal*

We address the problem of electronic and nuclear spin resonance of an individual atom on a surface driven by a scanning tunneling microscope. Several mechanisms have been proposed so far, some of them based on the modulation of exchange and crystal field associated with a piezoelectric displacement of the adatom driven by the radio frequency (RF) tip electric field. Here we consider another mechanism, where the piezoelectric displacement modulates the *g*-factor anisotropy, leading both to electronic and nuclear spin flip transitions. We discuss thoroughly the cases of hydrogenated Ti ($S = 1/2$) and Fe ($S = 2$) on MgO, relevant for recent experiments. We model the system using two approaches. First, an analytical model that includes crystal field, spin orbit coupling, and hyperfine interactions. Second, we carry out density-functional-based calculations. We find that the modulation of the anisotropy of the *g* tensor due to the piezoelectric displacement of the atom is an additional mechanism for scanning tunneling microscopy (STM)-based single spin resonance that would be effective in $S = 1/2$ adatoms with large spin orbit coupling. In the case of hydrogenated Ti on MgO, we predict a modulation spin resonance frequency driven by the DC electric field of the tip.

I. INTRODUCTION

The quest of single spin electron paramagnetic resonance (EPR) driven with a scanning tunneling microscope (STM) has been pursued for many years [1,2]. The first report of STM-EPR of individual adatoms on a surface of MgO(100)/Ag [3] has been followed by several dramatic breakthroughs in the study of spin physics of individual magnetic atoms [4–13]. This technique permits one to carry out absolute measurements of the magnetic moment of individual atoms [4,5]. The spectral resolution achieved so far, down to a few MHz, has made it possible to resolve the hyperfine structures of Fe, Ti, and Cu atoms [8,10]. In the case of Cu adatoms, the electrical driving of nuclear spin flip transitions that preserve the electronic spin has been demonstrated as well [10]. Thus, STM-EPR permits one to drive the electronic and nuclear spins of individual atoms on surfaces, as well as artificially created structures, such as dimers [6,9]. Importantly, the STM-EPR technique is being now implemented in several different laboratories, at higher temperatures [14] and higher driving frequencies [15].

An important question in the STM-EPR context [3–12], and also for experiments reporting electric control of individ-ual nuclear spin in single molecule transport [16,17], is the understanding of how electric fields couple both to electronic and nuclear spin degrees of freedom. This question has also been addressed in other systems. The idea of electric dipole spin resonance was proposed in 1960 by Rashba [18]. Electrical control of spin qubits has been reported in semiconductor nanostructures, based both on modulation of the *g* factor [19] and on inhomogeneous magnetic fields [20,21]. Electric fields have been used to drive spin resonance of itinerant electrons in InSb [22] and localized magnetic dopants in ZnO [23].

In the seminal paper of Baumann *et al.* [3], where a STM-EPR experiment was carried out with Fe atoms on an MgO surface, a mechanism was proposed to account for the coupling of the STM voltage to the *electronic* spin that depended on the specific details of the microscopic Hamiltonian of that system. The mechanism is based on the assumption that the radio frequency (RF) field induces a vertical piezoelectric displacement of the adatom, $\delta z \propto eV_{\rm RF}$, that in turns modifies the crystal field Hamiltonian of the *d* orbitals of Fe. This modulation, together with spin orbit coupling and a strong in-plane Zeeman field, would lead to spin transitions between the two lowest energy states of the $S = 2$, $S_z = \pm 2$ of Fe, a non-Kramers doublet integer spin system [24].

Other mechanisms have been proposed to account for the driving of the surface spin by the tip bias voltage [2,25–28]. For instance, in Ref. [26] we proposed a mechanism based on the modulation of the exchange interaction between the magnetic tip and the magnetic adatom that originates also from the piezoelectric distortion of the adatom.

Here we propose another complementary mechanism, that can coexist with the others, based on the electric modulation of the *g* tensor associated with the piezoelectric distortion of

---

*Corresponding author: aferron@gmail.com
†On leave from Departamento de Fisica Aplicada, Universidad de Alicante, 03690, Spain.

the adatom. As in the case of the crystal field [3] and exchange [11,26] mechanisms, we also assume that the magnetic adatom undergoes a piezoelectric displacement. In turn, this modulation changes the crystal field parameters that control the anisotropy of the electronic spin interactions that leads to an anisotropic *g* factor and to a renormalization of the hyperfine coupling. As we show below, these modulations lead both to electronic and nuclear spin flip transitions.

The rest of this paper is organized as follows. In Sec. II, we present a general argument to show that an anisotropic time-dependent modulation of the *g* tensor of a $S = 1/2$ system leads to electronic spin transitions. In Sec. III, we briefly present a single-particle Hamiltonian for a d^1 adatom with C_4 symmetry, valid for hydrogenated Ti (Ti-H) adatom on the oxygen site of MgO(001). In Sec. IV, we present our description of the Ti-H adatom on MgO based on density functional theory (DFT) calculations and how this connects with the crystal field Hamiltonian presented in the previous section.

In Sec. V, we derive analytical expressions for the *g* tensor anisotopy of Ti-H on MgO, based on the model of Sec. III. The *g* tensor obtained depends on the Ti spin orbit coupling and the crystal field parameters that can be obtained from DFT. In Sec. VI, we discuss how the *g* factor can be modulated for Ti-H on MgO by application of an electric field between tip and surface and we compute the associated Rabi energy. In Sec. VII, we briefly present the analogous piezoelectric modulation for Fe on MgO. In Sec. VIII, we discuss how the contact hyperfine interaction become anisotropic due to the *g*-factor anisotropy and how the *g*-factor modulation could induce nuclear spin flip transitions. In Sec. IX, we discuss the role of both the *g* tensor anisotropy of the adatom and the magnetic anisotropy of the tip in the efficiency of the exchange modulation [26] mechanism. In Sec. X, we show that the DC component of the tip-surface electric field induces a shift of the transition energy of the adatom due to the modification of the *g* tensor. Finally, in Sec. XI, we present some limitations of our models and we list our main conclusions. The Appendixes describe technical steps of some results used in the main text.

II. SPIN TRANSITIONS DRIVEN BY ANISOTROPIC MODULATION OF THE *g* TENSOR

For a free electron in vacuum, the interaction with a magnetic field is perfectly isotropic, in the sense that the energy splitting is the same regardless of the direction of the magnetic field $\vec{B}$. This results leads to the isotropic Zeeman interaction, $g\mu_B \vec{S} \cdot \vec{B}$. In contrast, for a general class of systems, the interplay between the spin orbit coupling $\vec{\ell} \cdot \vec{S}$, the orbital coupling to the magnetic field $\vec{\ell} \cdot \vec{B}$, and the crystal field splitting leads to an anisotropic Zeeman interaction. For instance, in the case of $S = 1/2$ adatoms, such as Ti-H [6,8–11] and Cu [10] on a 001 MgO surface, the interplay between the spin orbit coupling and the crystal field splitting leads to an anisotropic Zeeman interaction with different off-plane (z) and in-plane xy [29]:

$$\mathcal{H}_Z = g_x \mu_B B_x S_x + g_z \mu_B B_z S_z = \mu_B \vec{b}_0 \cdot \vec{S}, \qquad (1)$$

where $\vec{b}_0 = (g_x B_x, 0, g_z B_z)$.

As we show below, the tip *ac* electric field modulates the g_x and g_z coefficients, resulting in a time-dependent perturbation:

$$\mathcal{V}(t) = (\delta g_x \mu_B B_x S_x + \delta g_z \mu_B B_z S_z)\cos(2\pi f t). \qquad (2)$$

This equation can be written down as

$$\mathcal{V}(t) = \cos(2\pi f t)\mu_B \vec{b}_1 \cdot \vec{S}, \qquad (3)$$

where $\vec{b}_1 = (\delta g_x B_x, 0, \delta g_z B_z)$. This perturbation can induce spin transitions between the two eigenstates of $\mathcal{H}_0$ if $\vec{b}_0$ and $\vec{b}_1$ are noncollinear, $|\vec{b}_1 \times \vec{b}_0| \neq 0$. This yields

$$\frac{\delta g_z}{g_z} \neq \frac{\delta g_x}{g_x}. \qquad (4)$$

Thus, the perturbation (2) induces spin transitions if the relative modulations of the *g* factor are *different*. If we express the perturbation Hamiltonian in the basis of eigenstates of $\mathcal{H}_Z |\pm\rangle = \pm\frac{\Delta_z}{2}|\pm\rangle$,

$$\mathcal{V}(t) = \Omega_g \cos(2\pi f t)(|+\rangle\langle -| + |-\rangle\langle +|), \qquad (5)$$

where the Rabi coupling Ω_g is given by particularly simple equation, derived in Appendix A,

$$\Omega_g = \frac{\Delta_z}{4}\sin 2\theta \left(\frac{\delta g_z}{g_z} - \frac{\delta g_x}{g_x} \right), \qquad (6)$$

where $\Delta_z \equiv \mu_B |\vec{b}_0|$ is the Zeeman splitting, then θ is the polar coordinate of $\vec{b}_0$ defined in Eq. (1) [see also Eqs. (A2), (A12), and (A13)]. From Eq. (6), we immediately infer that the Rabi coupling created by the modulation of the *g* factor scales linearly with the *magnitude* of the magnetic field and has a very strong dependence on its orientation relative to the normal of the surface.

III. A MODEL HAMILTONAN FOR Ti-H on MgO

We now consider a model that describes a single electron occupying a *d* shell with a crystal field splitting with C_4 symmetry for rotations in the *xy* plane around the *z* axis. This permits one to obtain closed analytical expressions for the *g* tensor in terms of the crystal field parameters and the spin orbit coupling. In addition, our DFT calculations, discussed below, show that the model provides a fairly good description of hydrogenated Ti adatoms on the oxygen site of an MgO surface, relevant for STM-EPR experiments [6,8–11].

Ti^{2+} on MgO has two electrons in the *d* shell, and our DFT calculations show it has $S = 1$, in contrast with the experimental results [6,8–11]. It has been proposed that the reason why Ti/MgO has $S = 1/2$ is because it chemisorbs a hydrogen atom [6]. Our DFT calculations back up this assumption [6]. They show that hydrogen sits on top of Ti, almost colinear with the oxygen-Ti line that goes perpendicular to the surface. In that geometry, the *s* orbital of H hybridizes both with d_{z^2} and *s* orbitals of Ti and forms a molecular bonding-antibonding pair that hosts two electrons. This leaves only a single electron in the *d* shell, that occupies the x^2-y^2 orbital, so that the Ti-H system effectively has $S = 1/2$. We use the following Hamiltonian for the outermost electron of a single $S = 1/2$ electron in a *d* shell, that includes crystal field terms, spin orbit coupling, and Zeeman interaction:

$$\mathcal{H}_0 = -|D|\ell_z^2 + F((\ell^{(+)})^4 + (\ell^{(-)})^4)$$
$$+ \lambda \vec{S} \cdot \vec{\ell} + \mu_B \vec{B} \cdot (g\vec{S} + \vec{\ell}). \qquad (7)$$
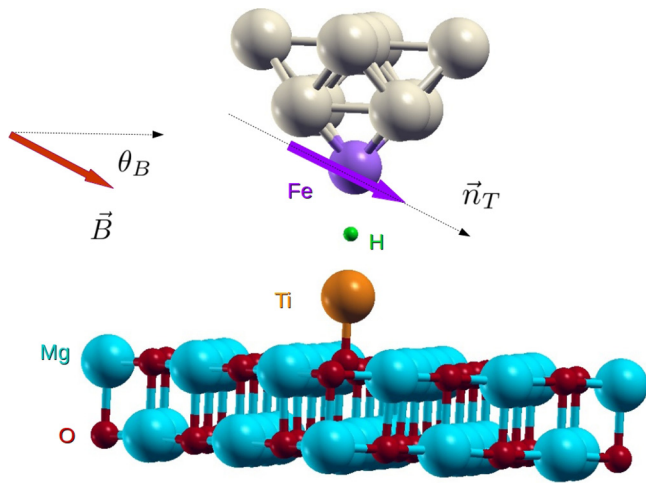
FIG. 1. Scheme of the STM-EPR experimental setup [3–12] with the atomic structure of Ti-H on the oxygen site of MgO. $\vec{B}$ is the external magnetic field applied during the experiment (with an angle θ_B measured with respect to the surface) and $\vec{n}_T$ shows the direction of the magnetic moment of the tip. Red balls represent O atoms, blue balls are Mg atoms, the violet ball is for the Fe atom, the green ball indicates the H atom, and the orange one is for the Ti atom.

Here, ℓ is the single particle angular momentum operator for the d electrons and $\vec{S}$ are the spin-1/2 matrices. Notice that Baumann *et al.* [3] used a mathematically similar expression for a multielectronic Hamiltonian multiplet with $L = S = 2$, valid for Fe on MgO. The crystal field terms account for the electrostatic interactions of the first neighbor charged ions of the Ti adatom (see Fig. 1). The Mg atoms are positively charged ions that reduce the energy of the xy and x^2-y^2 orbitals compared to the xz, yz, and z^2 orbitals. Oxygen atom is negatively charged and it increases the energy of the z^2 orbital. The D term accounts for these effects. In addition, the F term accounts for the C_4 symmetry of the surface and discriminates between the xy and x^2-y^2 orbitals, as one of them points toward the positively charged Mg ions, reducing the energy of that orbital, whereas the other points toward the oxygen atoms. The lowest energy orbital should be the x^2-y^2 [if we take the oxygen atoms in the (10) and (01) directions].

IV. DENSITY FUNCTIONAL CALCULATIONS FOR HYDROGENATED Ti

In this section, we focus on the electronic properties of individual hydrogenated Ti adatoms at MgO on top of oxygen, as described with density functional theory (DFT) calculations. With this aim, we have employed QUANTUM ESPRESSO [30], using projected augmented wave pseudopotentials, Perdew-Burke-Ernzerhof exchange correlation functional and 50–70 Ry of plane wave energy cutoff, as described elsewhere [30–32]. We performed calculations in a structure formed by a bilayer of MgO, as shown in Fig. 1, consisting of 36 O atoms (red balls) and 36 Mg atoms (blue balls) together with the hydrogenated Ti (orange ball) with one H (green ball). In order to check some results, we also performed a few number of calculations using a bigger supercell with 64 O atoms, 64 Mg atoms, and the hydrogenated Ti. The main
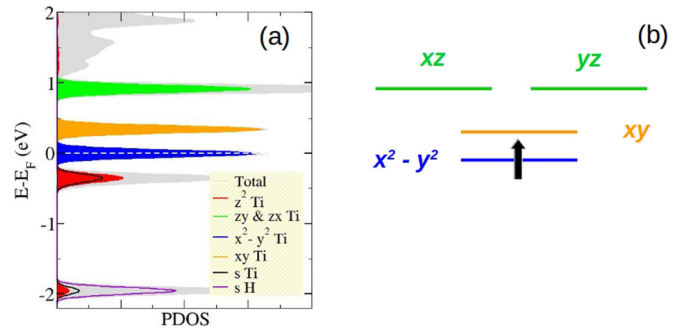

FIG. 2. (a) DFT calculations for the spin-unpolarized density of states projected over d and s orbitals of Ti and the s orbital of hydrogen. The gray shadow shows the total density of states. (b) Energy level cartoon.

distortions created by the adatom in the MgO bilayer are (i) an upward displacement of the closest oxygen(s) to adatoms and (ii) a downward distortion of the Mg atoms located below the Ti-bonded oxygen atoms. Our DFT calculations found that a hydrogenated Ti atom shows $S = 1/2$ [6,8]. The spin density of hydrogenated TiO (with the Ti and H atoms located collinear along the z axis) is consistent with a filling of the $d_{x^2-y^2}$ orbital, since we are assuming that the Mg atoms' first neighbor are in the x and y axes.

Figure 2(a) shows the projected density of states over d orbitals for the hydrogenated Ti at MgO on top of oxygen, computed with no spin polarization. DFT yields x^2-y^2 and a hybrid orbital z^2-s as the lowest energy orbitals, within the d manifold. The z^2 of the Ti d shell is strongly hybridized with the hydrogen $1s$ orbital. As a result, the z^2 and the s are split in energy and altogether host two electrons. The xy orbital comes next in energy and is empty. The orbital doublet xz and yz lies higher up in energy. Calculations show that x^2-y^2 hosts exactly one electron. It is apparent that the Hamiltonian model Eq. (7) with $\ell_z = \pm 1, \pm 2$ describes the four orbitals x^2-y^2, xy, xz, and yz.

A. Connection between DFT and model Hamiltonian

We now explain how to obtain a rough estimate of D and F parameters that enter in the crystal field Hamiltonian (7). The method amounts to fit the energy difference of the peaks in the density of states obtained from a spin-unpolarized DFT calculation to those obtained from Eq. (7):

$$E_{x^2-y^2} - E_{xy} = 48F, \tag{8}$$

$$2E_{xz} - E_{x^2-y^2} - E_{xy} = 6|D|, \tag{9}$$

Using these equations, from inspection of the density of states we infer the values $D \simeq -255$ meV and $F \simeq 7.50$ meV. This crude approximation is enough for the scope of this work.

We can also obtain an estimate for the modulation of the crystal field parameters, D and F, as the length of the Ti-O bond is changed from its equilibrium position. The calculation is carried out moving Ti atom and relaxing the four closest neighbor Mg atoms, the O atom below and the H atom, keeping all the others fixed. The results of the parameters D

and F, obtained with this procedure, allow us to obtain the following relation of D, F, and the strain:

$$\frac{dF}{dz} = -6\frac{\text{meV}}{\text{Å}}, \tag{10}$$

$$\frac{dD}{dz} = +188\frac{\text{meV}}{\text{Å}}. \tag{11}$$

These values are used later on to estimate how the piezoelectric displacement of the Ti-O bond modulates the crystal field values F and D that in turn modulate the g tensor.

B. Calculation of the *g* tensor from DFT

We have calculated the g tensor components from our DFT calculations using gauge including projector augmented waves (GIPAW). GIPAW is a DFT-based method to calculate magnetic resonance properties [33], where spin orbit coupling is implemented in a perturbative way. Our calculations for the structure in equilibrium $\delta z = 0$ give us a diagonal g tensor with components $g_x = g_y = 1.974$ and $g_z = 1.881$. As we discuss now, the model Hamiltonian Eq. (7) provides physical insight on the origin of the anisotropy and very good agreement with the values obtained from DFT.

V. CALCULATION OF THE *g* TENSOR FROM THE MODEL

We now use the model Hamiltonian Eq. (7) to compute the g tensor. We do this at two levels of approximation. First, we obtain analytical approximate expressions from the model Hamiltonian. Second, we obtain the g tensor from the exact numerical solution of the model. Both the analytical and numerical approaches permit us to relate the g-tensor components with the crystal field parameters D and F and the spin orbit coupling λ. On account of the C_4 symmetry of the Hamiltonian, the g tensor is diagonal and has $g_x = g_y$. Therefore, we only need to compute g_z and g_x.

A. Calculation of g_z

We first consider the response of the electron in the x^2-y^2 state to a magnetic field in the z direction. For that matter, we need to consider the space of four states with $\ell_z = \pm 2$ and $S_z = \pm 1/2$. Within this subspace, spin orbit coupling only acts through the $S_z \ell_z$ term. Therefore, S_z is conserved, and the Hamiltonian for each S_z is given by

$$\mathcal{H}_{S_z}(B_z) = \begin{pmatrix} -\lambda \ell_z S_z + \Delta_-(B_z) & 24F \\ 24F & \lambda \ell_z S_z + \Delta_+(B_z) \end{pmatrix}, \tag{12}$$

where $\Delta_\pm(B_z) = \mu_B B_z(gS_z \pm \ell_z)$ with $\ell_z = 2$. Hamiltonian Eq. (12) can be written as

$$\mathcal{H}(S_z) = g\mu_B B_z S_z + \vec{h}(S_z) \cdot \vec{\sigma}, \tag{13}$$

where

$$\vec{h}(S_z) = [24F, 0, -\ell_z(\mu_B B_z + S_z \lambda)]. \tag{14}$$

We thus have $\epsilon_2(S_z, \pm) = -4|D| + E^{(\pm)}(S_z)$, where

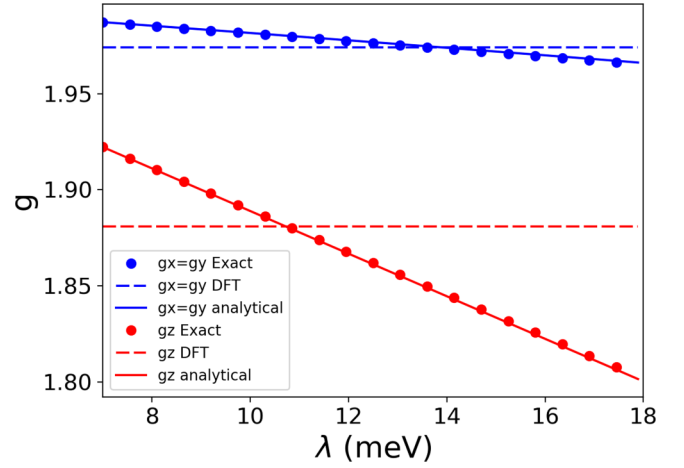$$E^{(\pm)}(S_z) = g\mu_B B_z S_z \pm \sqrt{(24F)^2 + \ell_z^2(\mu_B B_z + S_z \lambda)^2}.$$

FIG. 3. Dependence of g_x and g_z on spin orbit coupling λ, for Ti-H on oxygen, obtained in two ways: solution of full model Eq. (7) with $D = -255$ meV and $F = 14$ meV (symbols) and using analytical results ignoring $\ell_z \neq 2$ manifolds [Eqs. (15) and (22)] (lines). DFT results are shown for reference as dashed lines.

We now Taylor expand the ground state of the E^- states around $B_z = 0$:

$$E^{(-)}(S_z) = -\sqrt{(24F)^2 + \lambda^2} + g\mu_B S_z B_z + \delta g_z S_z \mu_B B_z,$$

where

$$g_z = g + \delta g_z = 2 - \frac{4\lambda}{\sqrt{(24F)^2 + \lambda^2}}. \tag{15}$$

Interestingly, there are no higher order corrections to δg_z, coming from mixing with the $\ell_z = \pm 1$ manifold. This is confirmed by the comparison of Eq. (15) with the results obtained from exact diagonalization of the complete model (7). As a result, we can use Eq. (15) for obtain the ratio $\frac{F}{\lambda} = 1.4$ that gives g_z, in agreement with the DFT result $g_z = 1.881$ The dependence of g_z on λ, F, and D is shown in Fig. 3. Note that, as shown in Fig. 4, g_z does not depend on D and we can use $F/\lambda = 1.4$ to ensure that $g_z = 1.881$.

B. Calculation of g_x

We now obtain an analytical expression for g_x for the x^2-y^2 ground-state manifold of Hamiltonian Eq. (12). For that matter, we represent the operator $\mu_B B_x(gS_x + \ell_x)$ in the basis of eigenstates of $\mathcal{H}(\sigma)$:

$$|\psi_-(\uparrow)\rangle = \cos\frac{\alpha}{2}|-2, \uparrow\rangle - \sin\frac{\alpha}{2}|+2, \uparrow\rangle,$$

$$|\psi_-(\downarrow)\rangle = \cos\frac{\alpha}{2}|+2, \downarrow\rangle - \sin\frac{\alpha}{2}|-2, \downarrow\rangle,$$

where the angle α is defined as

$$\vec{h}(S_z) = |\vec{h}(S_z)|(\sin\alpha(S_z), 0, \cos\alpha(S_z)) \tag{16}$$

and $\vec{h}$ is defined in Eq. (14). In this subspace, the matrix elements of ℓ_x are zero and the only nonzero matrix element of S_x reads

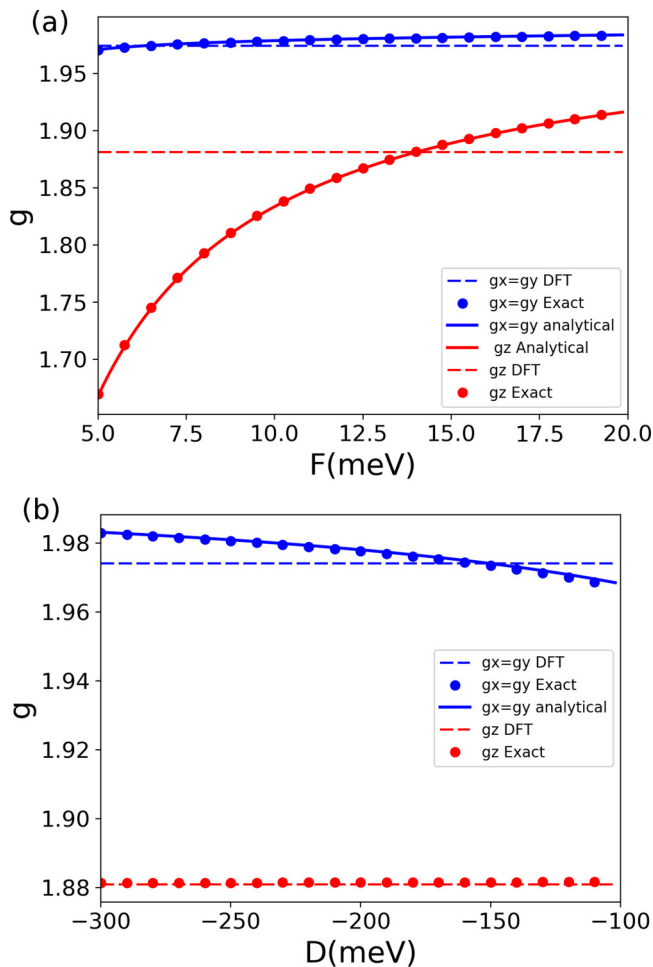$$\langle\psi^-(\uparrow)|S_x|\psi^{(-)}(\downarrow)\rangle = -\frac{1}{2}\sin\alpha. \tag{17}$$

FIG. 4. Dependence of g_x and g_z on crystal field parameters F (a) and D (b) for Ti-H on oxygen, obtained from full model Eq. (7) (solid points in both panels), DFT (dashed lies), and analytically (solid lines) [Eqs. (15) and (22)]. In both panels, we take $\lambda = 10$ meV. (a) $D = -255$ meV. (b) $F = 14$ meV.

For $B_z = 0$, we have

$$\sin \alpha = \frac{24F}{\sqrt{(24F)^2 + \lambda^2}}, \quad \cos \alpha = \frac{-|2S_z|\lambda}{\sqrt{(24F)^2 + \lambda^2}}. \quad (18)$$

Thus, the eigenvalues of the Hamiltonian are

$$\epsilon_2(B_x) = -3|D| - \sqrt{(24F)^2 + \lambda^2} \pm \frac{g}{2}\mu_B B_x \sin \alpha. \quad (19)$$

We thus have

$$g_x^{(1)} = g \sin \alpha = g \frac{24F}{\sqrt{(24F)^2 + \lambda^2}}. \quad (20)$$

We now consider the contributions to g_x that arise from the virtual transitions to the $\ell = \pm 1$ levels. These are driven by the combined action of the $\mu_B \ell_x B_x$ and the flip-flop part of the spin orbit interaction. This additional contribution gives

$$\delta g_x^{(2)} = -\frac{2\lambda}{3|D| + 24|F| + |\lambda|} \quad (21)$$

so that the g_x factor is given by

$$g_x = g \frac{24F}{\sqrt{(24F)^2 + \lambda^2}} - \frac{2\lambda}{3|D| + 24|F| + |\lambda|}. \quad (22)$$

The anisotropy of the g tensor arises ultimately from the fact that the $\ell_z = \pm 2$ states have a strong additional orbital response only when B is applied in the z direction. This extra contribution is quenched by the F crystal field term that leads to states with equal weight on the two $\ell_z = \pm 2$ states but promoted by the spin orbit coupling. The resulting anisotropy is thus controlled by the competition between λ and F. In addition, g_x has also a contribution that arises from virtual coupling to the $\ell_z = \pm 1$ states. For the values of D, F, λ adequate to describe Ti-H on MgO, the dominant contribution to the deviation of g_x from the value $g = 2$ arises from the virtual coupling to $\ell = \pm 1$.

So, for $F = 0$ we have $g_x^{(1)} = 0$, because the spin orbit coupling correlates S_z and ℓ_z so that spin flips entail momentum flips that are forbidden, and $g_z = -2$ because of the dominant orbital contribution. In the opposite limit of $\lambda = 0$, we recover $g_x = g_z = 2$. If we repeat the analysis for g_y, we obtain $g_x = g_y$, as expected from the C$_4$ surface's symmetry.

In Figs. 3 and 4, we show the predictions for g_x and g_z, as functions of λ, D, and F, obtained using both the analytical formulas Eqs. (15) and (22) and the exact solution of the complete Hamiltonian Eq. (7). The DFT results are shown as dashed horizontal lines. In Figs. 3 and 4(a) we take $D = -255$ meV, roughly estimated from DFT, using Eq. (9), which gives a single particle spectrum, in agreement with the results of DFT. In Fig. 4(b), we take $\lambda = 10$ meV and $F = 14$ meV, also inferred from comparison with DFT. In Fig. 4, we fix $\lambda = 10$ meV and $F = 1.4\lambda$ so that we obtain values very close to those obtained with DFT. Finally, Fig. 4(b) shows that the dependence of g_x on D is small and g_z does not depend on D.

Summing up, the results of this section show how, for a model with the symmetry adequate for a TiH on top of an oxygen on an (001) MgO surface, the g factor is anisotropic, $g_z \neq g_x = g_y$, and how g_z and g_x depend on the crystal field parameters F, and to a lesser extent, on D. Our analytical model is able to give g_x and g_z, in agreement with the values obtained from DFT.

VI. PIEZOELECTRIC MODULATION OF g FOR Ti-H on MgO

We have shown that a modulation of the g-factor anisotropy would induce spin-flip transitions [Eq. (6)], and we have computed how the g-factor components depend on the crystal field parameters F and D. We now argue that an electric field applied perpendicular to the surface of MgO modulates F and D, and thereby the g-factor anisotropy, resulting in spin transitions between the two states of the lowest energy Kramers doublet of Eq. (7).

Our DFT calculations show that crystal field parameters D and F are functions of the adatom-oxygen distance, z: $D(z), F(z)$ [see Eqs. (10) and (11) and Fig. 5]. We denote the equilibrium position by z_{eq}. The electric field across the gap between the STM and the MgO surface, $E = V_{\text{tip}}/d$, where d is the tip-MgO distance, induces a force on the adatom, $F = q_{\text{adatom}}V_{\text{tip}}/d$ on account of its charge q_{adatom} [3,11,26]. This
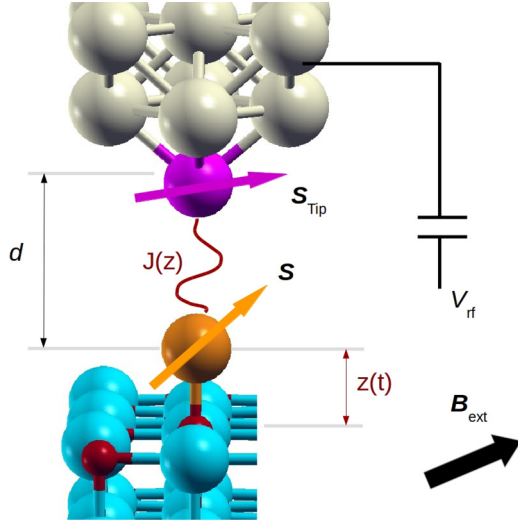
FIG. 5. Schematic showing a magnetic atom (orange) on MgO and an Fe atom (violet) attached to the apex of the STM tip. The solid (orange and violet) arrows indicate the orientations of the respective magnetic moments ($\vec{S}$ and $\vec{S}_{\text{tip}}$). The exchange interaction J is indicated by the red curve and the piezoelectric displacement is represented with a red arrow. A radio-frequency voltage drives the ESR of the magnetic atom. The external magnetic field B_{ext} is applied out of the plane of the substrate (with a small angle).

force is compensated by a restoring elastic force $F = -k\delta z$. Thus, the adatom equilibrium position is displaced by [26]

$$\delta z(t) = \frac{q_{\text{adatom}} V_{\text{tip}}(t)}{kd}. \tag{23}$$

This equation is valid for a time-dependent V_{tip} as long as its Fourier components are away from the mechanical resonance frequency of the stretching mode, $\sqrt{\frac{k}{M}}$, where M is the mass of the adatom. According to our DFT calculations [11,26], this frequency is up in the THz range, as long as we ignore the contributions coming from the off-plane (flexural) phonons of the MgO. In the following, we assume $V_{\text{tip}}(t) = V_{\text{RF}}^0 \cos(2\pi f t)$ so that we have

$$\delta z(t) = \frac{q_{\text{adatom}} V_{\text{RF}}^0(t)}{kd} \cos(2\pi f t) \equiv \delta z_0 \cos(2\pi f t). \tag{24}$$

From our DFT calculations for Ti-H on MgO [11], we obtain $k = 290$ eV nm^{-2}, so that for RF tip voltages values ranging from $eV_{\text{RF}}^0 = 10$ meV to $eV_{\text{RF}}^0 = 20$ meV and $d = 5$Å, the piezoelectric displacement amplitude goes from $\delta z_0 = 0.07$ pm to $\delta z_0 = 0.14$ pm.

The modulation of crystal field parameters F and D with the Ti-O bond length leads to a modulation of the g tensor:

$$\delta g_a = \left(\frac{\partial g_a}{\partial F} \frac{\partial F}{\partial z} + \frac{\partial g_a}{\partial D} \frac{\partial D}{\partial z} \right) \delta z(t). \tag{25}$$

It must be noted that this equation is also valid in the DC limit.

We now proceed to estimate the magnitude of the Rabi coupling associated to the modulation of the g factor. We do that using two different methods that, as we discuss below, give the same result. The first method consists of using Eq. (6). In the second method, we evaluate directly the matrix elements
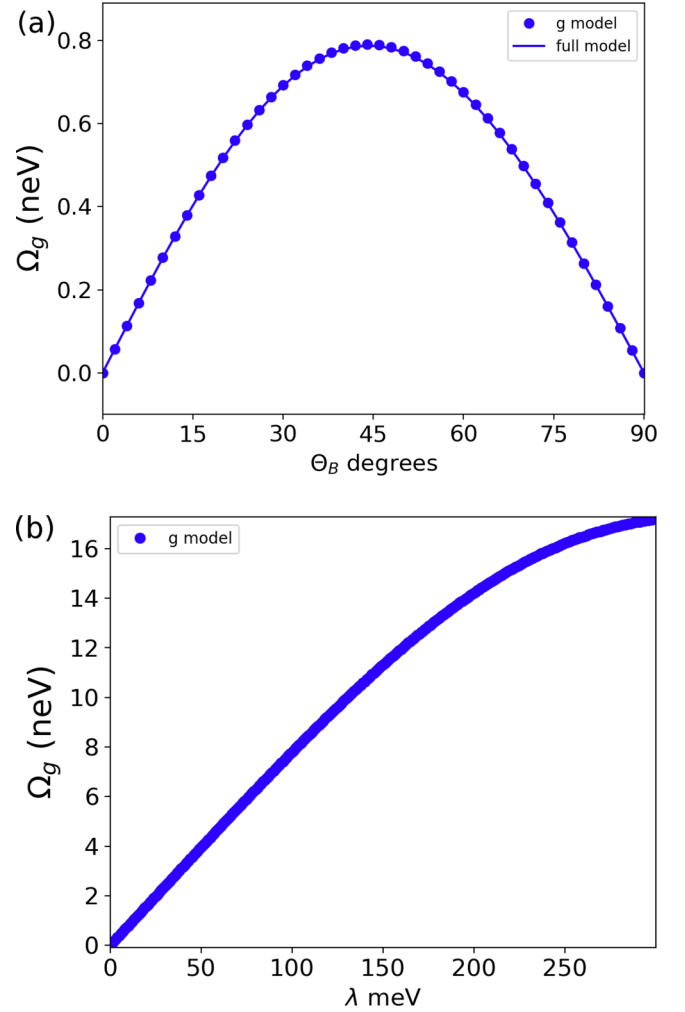

FIG. 6. (a) Rabi coupling due to g-factor modulation as a function of the angle θ_B between $\vec{B}$ and surface calculated with two methods: Eqs. (6) and (27). $\lambda = 10$ meV, $F = 1.4\lambda = 14$ meV, $D = -255$ meV, $B = 1T$, $V_F = 20$ meV, STM-surface distance $d = 5$Å, $k = 290$ eV/nm^2. (b) Dependence of Ω_g on λ, keeping all the other constants the same and $\theta_B = 45$ deg.

of the crystal field operators, using the same approach used in previous works [3,26].

A. Rabi coupling from the g-factor anisotropy

In order to compute the Rabi coupling from Eq. (6), we need to compute Eq. (25). For that matter, we obtain $\frac{\partial g_a}{\partial F}$ and $\frac{\partial g_a}{\partial D}$ from our model Hamiltonian, and we use $\frac{\partial F}{\partial z}$, $\frac{\partial D}{\partial z}$ calculated from DFT calculations in Sec. IV A.

We are now in position to estimate Ω_g, combing Eqs. (6), (10), (24), and (25). We now take $V_{\text{RF}}^0 = 20$ meV, $d = 5$ Å, and $k = 290$ eV/nm^2 (taken from DFT calculations). This yields a strain of the Ti-O distance of $\delta z_0 = 0.14$ pm. In Fig. 6(a), we plot the magnitude of the Rabi coupling so obtained, as a function of the angle between the magnetic field and the surface, θ_B for $B = 1$ Tesla. The first thing to note is that the magnitude of Ω_g is between one and two orders of magnitude smaller than the experimental values reported in our previous work [11]. Therefore, other mechanism, most

likely exchange modulation [26], has to be involved in the electric field driving of the spin for EPR-STM for Ti-H/MgO.

The magnitude of Ω_g scales linearly both with the applied field B and with the RF electric field $\frac{V_{RF}}{d}$. The optimal angle to maximize Ω_g is close to 45 deg. In contrast, the exchange mechanism is independent of B and scales exponentially [11] with d. Whereas the g-factor modulation is not dominant for Ti-H on MgO, it could be the dominant factor in heavier adatoms. To show this, in the bottom panel of Fig. 6(b) we plot Ω_g ramping λ, keeping all the other parameters the same and taking $\theta_B = 45$. It is apparent that, for a wide range, Ω_g scales linearly with spin orbit coupling. Expectedly, Ω_g vanishes for $\lambda = 0$, as the g-factor anisotropy is driven by λ.

B. Rabi coupling from crystal field matrix elements

We now carry out a sanity check. Given that the electronic spin flip transitions described by the effective $S = 1/2$ model of Eqs. (1) and (2), arise ultimately from the modulation of the crystal field operators of the parent Hamiltonian of Eq. (7), we have computed the Rabi coupling using the parent model as well. To do so, we first obtain the two lowest eigenstates of Hamiltonian from Eq. (7), $\mathcal{H}|\pm\rangle = (E_g \pm \frac{\Delta_z}{2})|\pm\rangle$ and we then compute the matrix elements of the perturbation operator:

$$\mathcal{V}(t) = \frac{\partial D}{\partial z}\delta z(t)\ell_z^2 + \frac{\partial F}{\partial z}\delta z(t)[(\ell^{(+)})^4 + (\ell^{(-)})^4], \quad (26)$$

where the time dependence is described by Eq. (24). We thus define

$$\Omega_{CF} = \frac{\partial D}{\partial z}\delta z_0\langle+|\ell_z^2|-\rangle$$
$$+ \frac{\partial F}{\partial z}\delta z_0\langle+|[(\ell^{(+)})^4 + (\ell^{(-)})^4]|-\rangle. \quad (27)$$

The results of the calculation of Ω_{CF} as function of θ_B, obtained with the same values of λ, D, F, d, V_{RF}, k, and B of the previous subsection, are shown in Fig. 6 and, expectedly, are in full agreement with those obtained using Eq. (6). This agreement validates our analysis.

VII. *g*-FACTOR MODULATION OF Fe on MgO

The results of the last paragraph show that it is possible to interpret the modulation spin driving coming from the modulation of the crystal field parameters [Eq. (27)] in terms of a modulation of the g factor [Eq. (6)]. In the seminal work of Baumann *et al.* [3], the modulation of the crystal field (CF) was proposed as the driving mechanism for EPR-STM of Fe/MgO. Here we address the question of whether we can recast the CF mechanism in terms of the g-factor modulation, for the case of Fe on MgO as well.

In order to find the answer, that turns out to be negative, we need to model the g-factor modulation for Fe on MgO and to compare with the results obtained from the CF modulation. The main difference with the case of Ti-H is that the ground state of Fe on MgO has $S = 2$. Therefore, a multielectronic description is necessary [3,26,34].

We follow our own work [26] and we model Fe on MgO with a two levels of complexity. First, a microscopic Hamiltonian for six electrons in the d orbitals of Fe, in the presence of

a crystal field, spin orbit coupling, Coulomb interaction, and Zeeman interaction:

$$\mathcal{H}_{Fe} = H_{CF} + H_{SOC} + H_Z + V_{ee}. \quad (28)$$

The single particle crystal field Hamiltonian reads

$$\mathcal{H}_{CF} = D\ell_z^2 + F(\ell_x^4 + \ell_y^4). \quad (29)$$

As explained in Appendix C, this CF Hamiltonian turns is almost identical to the one we have used in Eq. (7) Ti-H/MgO. As we did in the case of Ti-H/MgO, we can infer D and F from DFT calculations [26]. For $z = z_{eq}$ we obtain, from DFT calculations, $F = -10$ meV and $D = -290$ meV [26]. The spin orbit coupling constant for Fe is $\lambda = 35$ meV [26].

The many-body Hamiltonian can be solved exactly, by numerical diagonalization in a space made with all the states that accommodate six electrons in five spin-degenerate d orbitals. The lowest energy manifold has five states, corresponding to a ground state with $S = 2$ and can be described in terms of an effective spin model:

$$H_{eff} = -\mathcal{D}_2 S_z^2 + \mathcal{D}_4 S_z^4 - \mathcal{F}(S_+^4 + S_-^4) + \mu_B \mathbf{B} \cdot g \cdot \mathbf{S}, \quad (30)$$

where the spin operators act on the $S = 2$ subspace. The main difference with the $S = 1/2$ case is the presence of single-ion anisotropy terms. The anisotropy terms $\mathcal{D}_2$, $\mathcal{D}_4$, $\mathcal{F}$, and the g tensor can be obtained from the diagonalization of Hamiltonian Eq. (28). We obtain $\mathcal{D}_2 = 4.9$ meV, $\mathcal{D}_4 = 0.23$ meV, and $\mathcal{F} = 11$ neV. With these numbers, the spectrum of the $S = 2$ manifold has a EPR active space formed by a doublet of states with $S_z = \pm 2$, that we denote as $|0\rangle$ and $|1\rangle$. Yet, this doublet is fundamentally different [24] from the $S = 1/2$ Kramers pair, as it has a zero field splitting, given by $\Delta = 48\mathcal{F} = 0.5$ μeV, due to quantum spin tunneling [35–38]. Thus, the EPR active doublet for Fe on MgO cannot be described in terms of a Zeeman-only Hamiltonian. At $B = 0$, none of the two lowest energy states has a magnetic moment [38]. However, application of a modest off-plane field is enough to induce an off-plane magnetic moment in the two lowest energy states, on account of the small value of Δ.

Diagonalizations of the multielectronic Hamiltonian Eq. (28) at finite magnetic field permit us to derive the g tensor. Expectedly for a system with C_4 symmetry, it is diagonal in the Cartesian basis. The values of the g tensor do depend on the single particle crystal field parameters D and most notably on F and λ. For the values quoted above, we obtain $g_z = 2.8$ and $g_x = g_y = 2.0$.

Importantly, all the constants in the effective Hamiltonian Eq. (30) do depend strongly on the single particle crystal field parameter F that in turns depends on the piezoelectric displacement [26]. Following an argument similar to the one used for d^1 atoms, we can calculate the Rabi frequency derived from the effective Hamiltonian. We break it down in two types of terms:

$$\Omega_{eff} = \Omega_{ZFS} + \Omega_g. \quad (31)$$

The first comes from the modulation of the zero field energy constants, $\mathcal{D}_2$, $\mathcal{D}_4$, and $\mathcal{F}$ and was absent in the case of $S = 1/2$ adatoms. The dominant contributions [26] arise from the modulation of the F term in the single particle crystal field of
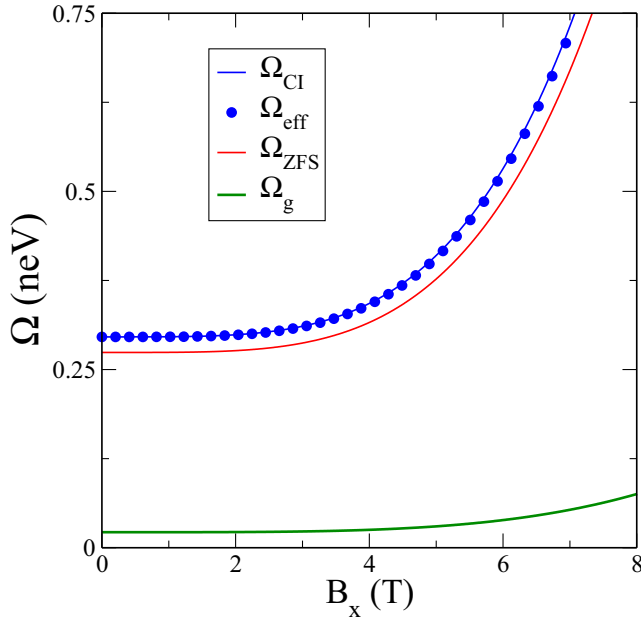
FIG. 7. Breakdown of Rabi coupling for Fe on MgO as a function of in-plane magnetic field B_x. The calculation were performed for $B_z = 0.2$ T, $k = 600$ eV/nm^2, $d = 0.6$ nm, $V_{RF} = 8$ mV, $D = -290$ meV, $F = -10$ meV, $\lambda = 35$ meV, and $q = 2e$.

Eq. (29):

$$\Omega_{ZFS} = \left(-\frac{\partial \mathcal{D}_2}{\partial F} \langle 0|S_z^2|1\rangle + \frac{\partial \mathcal{D}_4}{\partial F} \langle 0|S_z^4|1\rangle \right.$$
$$\left. - \frac{\partial \mathcal{F}}{\partial F} \langle 0|S_+^4 + S_-^4|1\rangle \right) \frac{\partial F}{\partial z}, \quad (32)$$

where $\frac{\partial F}{\partial z} = 280$ meV/nm, obtained from DFT in a previous publication [26]. The second class of contribution to the Rabi coupling comes from the g-factor modulation, very much like the $S = 1/2$ case:

$$\Omega_g = \mu_B \left(\frac{\partial g_z}{\partial F} B_z \langle 0|S_z|1\rangle + \frac{\partial g_x}{\partial F} B_x \langle 0|S_x|1\rangle \right) \frac{\partial F}{\partial z}. \quad (33)$$

We can assess the relative contribution of the zero field splitting and the g-tensor modulations in the following way. We first compute the Rabi coupling using the whole multielectron Hamiltonian [26] and we refer to this as Ω_{CI}. The calculation, done for $B_z = 0.2$ T, $k = 600$ eV/nm^2, $d = 0.6$ nm, $V_{RF} = 8$ mV, $D = -290$ meV, $F = -10$ meV, $\lambda = 35$ meV, and $q = 2e$ is shown in Fig. 7 as a function of the in-plane field B_x, together with the different contributions, Ω_{ZFS} and Ω_g, computed using the effective Hamiltonian Eqs. (30), (32), and (33). It is apparent that the $\Omega_{CI} = \Omega_{ZFS} + \Omega_g$, which validates our methods.

Importantly, our calculations show that the modulation of the g factor is not a dominant contribution to the spin transitions driven by the modulation of the crystal field parameter F due to off-plane piezoelectric distortion of the adatom. In addition, it was found in Ref. [26] that the exchange modulation mechanism is probably dominant for Fe. Therefore, the g-factor modulation plays a marginal role in the case of Fe.

VIII. MODULATION OF THE HYPERFINE INTERACTION

Here we briefly address how the modulation of the g-factor anisotropy affects the hyperfine interaction. Recently, electrical control of an individual nuclear spin of $S = 1/2$ Cu atom was demonstrated using STM-EPR [10]. For simplicity, here we consider the case of Ti-H on MgO, for which hyperfine splittings have been observed experimentally [8]. We consider a simplified hyperfine model where only the contact interaction term is considered:

$$\mathcal{V}_{HF} = A\mathbf{I} \cdot \mathbf{S}. \quad (34)$$

For simplicity, the dipolar and quadruple terms are neglected, although they are known to be relevant for Ti-H on MgO [8]. We now address how the modulation of the g-factor anisotropy affects this Hamiltonian and we find that the effective hyperfine coupling becomes anisotropic.

For that matter, we consider the representation of the isotropic hyperfine operator Eq. (34) in the basis set defined by the tensor product of the lowest energy eigenstates of Hamiltonian Eq. (7), whose wave functions are given by Eq. (16), and the eigenstates of the nuclear spin operator I_z. The resulting Hamiltonian reads

$$\mathcal{H}_{HF} = A_\parallel I_z S_z + A_\perp (I_x S_x + I_y S_y), \quad (35)$$

where

$$A_\parallel = A, \quad A_\perp = A \sin\alpha = A \frac{24F}{\sqrt{(24F)^2 + \lambda^2}}, \quad (36)$$

where F and λ are the crystal field and spin orbit coupling in Eq. (7). It is apparent that the modification of the hyperfine interaction is connected to the g-factor anisotropy.

We now discuss how the modulation of the g factor could lead to nuclear spin transitions that preserve the electronic spin. We consider the situation where a magnetic field induces an electronic Zeeman splitting so that the eigenstates of the electronuclear Hamiltonian can be split in two groups, according to their electronic spin [10]. We are interested in transitions between the low-energy manifold, so that initial and final states belong to the low-energy group, and only the nuclear spin changes in the transition. We thus consider transitions between two eigenstates that differ by single nuclear spin flip [10]:

$$|I_z\rangle_- = \sqrt{1 - \epsilon^2}|\downarrow\rangle|I_z\rangle + \epsilon|\uparrow\rangle|I_z - 1\rangle \quad (37)$$

and

$$|I_z - 1\rangle_- = \sqrt{1 - \epsilon^2}|\downarrow\rangle|I_z - 1\rangle + \epsilon|\uparrow\rangle|I_z - 2\rangle, \quad (38)$$

where $\epsilon \propto \frac{A_\perp}{g_z \mu_B B_z} \ll 1$. These states have a dominant $\downarrow$ electronic spin component and a small mixing due to the nonresonant spin-flip hyperfine interaction.

It is apparent that a perturbation that flips the electronic spin can induce transitions between these two states:

$$_-\langle I_z - 1|S^-|I_z\rangle_- \propto \epsilon\sqrt{1 - \epsilon^2} \simeq \frac{A_\perp}{g_z \mu_B B_z}, \quad (39)$$

showing the electronically driven nuclear spin transition matrix element is proportional to the hyperfine interaction. Thus, the same modulation of the g tensor that drives electronic spin

transitions, when f in the range of the electronic Zeeman transition, can also drive nuclear-spin flip transitions if f is in the range of the hyperfine interaction, as shown experimentally in the case of Cu on MgO [10].

We finally note that the modulation of F will in turn change $A_\perp$ providing a time-dependent electron-nuclear perturbation,

$$\delta \mathcal{V}_{\mathrm{HF}} = \delta A_\perp(t)\big(I_x S_x + I_y S_y\big), \qquad (40)$$

where $\delta A_\perp = \frac{\partial A_\perp}{\partial F}\frac{\partial F}{\partial z}\delta z(t)$. However, this electron-nuclear flip-flop operator cannot mix the states (37) and (38). The flip-flip modulation can induce EPR-like transitions, between state (37) and

$$|I_z - 1\rangle_+ = \sqrt{1-\epsilon^2}|\uparrow\rangle|I_z-1\rangle + \epsilon|\downarrow\rangle|I_z\rangle. \qquad (41)$$

This could be a relevant mechanism for EPR-STM in systems with very large hyperfine interaction, such as Bi in silicon [39] or perhaps Cu/MgO [11]. Hyperfine-driven electric spin dipole resonances have been reported in semiconductor quantum dots [40].

IX. ROLE OF ANISOTROPIC g FACTOR AND THE EXCHANGE-DRIVEN MECHANISM FOR EPR-STM

Although the main scope of this paper is to propose another mechanism for the electric field driving of the surface spins in STM-EPR, we briefly comment here on the role that the g-factor anisotropy plays on the exchange-modulation mechanism that we proposed in Ref. [26] and has been experimentally observed [11] for Ti-H adatoms on MgO. We now consider a Hamiltonian for the surface spin that, in addition to the Zeeman term, given by Eq. (1), has also exchange interaction with the tip. The magnetic moment of the tip is described semiclassically [11,26], so that the Hamiltonian for the surface spin reads

$$\mathcal{H}_{\mathrm{ex}} = \mathcal{H}_Z + J(z)\vec{n}_T \cdot \vec{S}, \qquad (42)$$

where (see Figs. 1 and 5)

$$\vec{n}_T = (\cos(\theta_B + \delta), 0, \sin(\theta_B + \delta)) \qquad (43)$$

describes the orientation of the tip moment, $\vec{B} = B_0(\cos(\theta_B), 0, \sin(\theta_B))$ is the external magnetic field forming and angle θ_B with the MgO surface as shown in Fig. 1 and $J(z)$ is the tip-adatom exchange interaction (Fig. 5) that depends on the tip-surface distance z.

In Appendix A 2, we derive an expression for the Rabi energy associated to the modulation δJ of the exchange formula:

$$\Omega_J = \mathcal{E}_J\left(\frac{\Delta g_x}{g} - \frac{\Delta g_z}{g}\right)\cos\theta_B \sin\theta_B \cos\delta$$
$$+ \mathcal{E}_J\left(1 + \frac{\Delta g_x}{g}\cos^2\theta_B + \frac{\Delta g_z}{g}\sin^2\theta_B\right)\sin\delta, \qquad (44)$$

where we write the ansotropic g factor as

$$g_x = g + \Delta g_x,$$
$$g_z = g + \Delta g_z, \qquad (45)$$

where Δg_x and Δg_z are the static contributions to the g-factor anisotropy,

$$\mathcal{E}_J \equiv \frac{\delta J}{2\Delta_z^*}g\mu_B B, \qquad (46)$$

and

$$\Delta_Z^* \equiv \sqrt{(g_x \mu_B B_x + J n_x)^2 + (g_z \mu_B B_z + J n_z)^2}. \qquad (47)$$

Let us consider now two different limits for this complicated formula. We study first the case $\delta = 0$, i.e., when the tip magnetic moment is aligned with the external magnetic field. This amounts to assume that the tip magnetic moment has an isotropic g factor. For $\delta = 0$, the exchange modulation Rabi splitting reads

$$\Omega_J = \frac{\mathcal{E}_J}{2}\sin 2\theta_B\left(\frac{\Delta g_x}{g} - \frac{\Delta g_z}{g}\right). \qquad (48)$$

Thus, this equation makes it apparent that the g-factor anisotropy of the surface spin is essential if the tip spin is aligned with B ($\delta = 0$). We note that, in spite of the similar aspect of Eqs. (6) and (48), they describe different mechanisms. In Eq. (6), the transitions are driven by the anisotropic modulation δg of the g-factor anisotropy. In Eq. (48), the transitions are driven by the modulation of the tip-surface spin δJ, but are enabled by the static g-factor anisotropy, given by Δg.

We now consider the case $\Delta g_x = \Delta g_z = \Delta g$, i.e., when the surface spin has an isotropic g factor. We obtain

$$\Omega_J = \mathcal{E}_J\left(1 + \frac{\Delta g}{g}\right)\sin\delta. \qquad (49)$$

Thus, the exchange-modulation Rabi depends on the misalignment angle between the tip moment and the applied field. In both cases, the exchange modulation Rabi splitting requires that either the tip or the surface spins, or both, have to be misaligned with respect to the applied field.

X. ELECTRIC CONTROL OF THE RESONANCE FREQUENCY

In the EPR-STM experiments, there is a DC bias, with amplitude V_{DC}, superimposed to the AC bias. In this section, we consider the shift of the resonance frequency of a $S = 1/2$ adatom with anisotropic g factor on account of the DC electric field between the tip and the surface. We consider the case of Ti-H/MgO. The underlying mechanism is the same that gives rise to the spin transitions: Application of an off-plane electric field induces a strain δz of the bond between the Ti adatom and the oxygen atom underneath [see Eq. (23)]. This leads to a modulation of the crystal field parameters D and F that in turn shifts the g tensor.

In the case of the g-factor modulation, we can obtain an expression for the shift of the resonance frequency for a given DC modulation δg_x and δg_z of the g tensor, up to linear order in Δg_a,

$$\hbar \delta \omega \simeq \mu_B^2 \frac{g_x \delta g_x B_x^2 + g_z \delta g_z B_z^2}{\Delta_z}, \qquad (50)$$

where Δ_z is the unperturbed modulation. We emphasize that δg_x and δg_z in Eq. (50) are the time-independent contributions
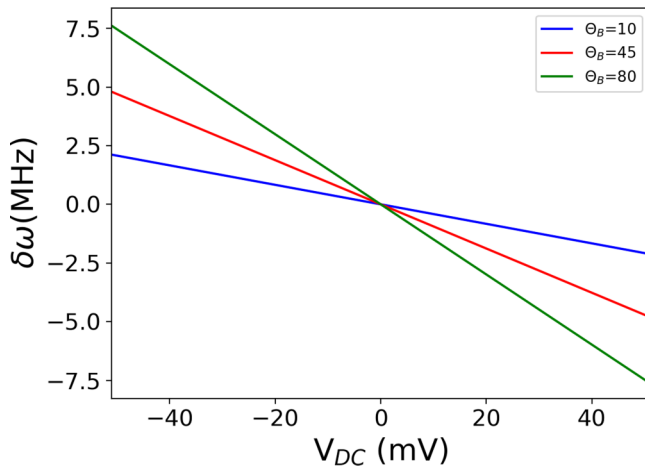
FIG. 8. Shift of the resonance frequency for $B = 1\,\text{T}$, $\lambda = 10\,\text{meV}$, $D = -255\,\text{meV}$, $F = 1.4\lambda\,\text{meV}$, $k = 290\,\text{eV/nm}^2$, and $d = 5\,\text{Å}$ for three different magnetic field angles.

to the g-factor anisotropy that arise from application of a DC electric field.

In Fig. 8, we plot the shift of the resonance frequency as a function of V_{DC} for a Ti-H adatom on MgO. The calculation is carried out with the Hamiltonian Eq. (7). We take $D = -255\,\text{meV}$, $F = 1.4\lambda = 14.0$ meV, and $B = 1\,\text{T}$. In order to compute δz, we take $k = 290\,\text{eV/nm}^2$ and a tip-MgO distance of $d = 5\,\text{Å}$ [11]. The shift scales inversely with d. We consider three orientations for $\vec{B}$, forming angles $\theta_B = 10°, 45°, 80°$. Expectedly, the resulting modulation is linear in V_{DC} and the effect is larger for fields off-plane, on account of the fact that $\Delta g_z > \Delta g_x$. With state of the art STM-EPR, the spectral resolution is around 3 MHz. Therefore, the shift might be observed for large values of V_{DC}.

The exchange with the tip also contributes to the shift in the EPR frequency [6,11,26]. Unlike the g-factor modulation mechanism, the exchange contribution is tip dependent and decays exponentially with d. Therefore, for larger tip-surface distance d, the g-factor modulation should dominate. Electric shift of the spin resonance was observed experimentally in bulk MgO doped with Cr [41], by means of conventional EPR.

XI. DISCUSSION AND CONCLUSIONS

The main idea of this paper is that electric fields can modulate the g-tensor anisotropy of magnetic adatoms, and that could be used to drive spin transitions. Our work comes motivated by recent EPR-STM experiments [3–12]. The electric modulation mechanism discussed here is an atomic scale version of the modulation of the g factor of electrons [19,42] and holes [43] in semiconductor nanostructures that lies at the heart of some well-known spintronics [44] and is becoming a resource in the manipulation of spin qubits [45,46]. At the atomic scale, the modulation proposed here occurs by controlling the weight of two orbital states with $\ell_z = \pm 2$ that have different orbital couplings.

We now briefly discuss some points of our work that could be improved. The derivation of the crystal field parameters for Ti-H/MgO could be improved using a Wannierization

[26,47]. In addition, we could also improve the model Eq. (7) by including the effects of hybridization between the d orbitals of Ti and the p and s orbitals of oxygen and s orbitals of titanium and hydrogen, as well as the effect of charge fluctuations [48].

Our estimation of the piezoelectric stretching could be improved in several ways. First, we are treating the silver substrate and most of the MgO as completely rigid. We have verified that keeping the MgO layer completely rigid, or letting a few atoms of the MgO layer close to the Ti adatom relax, has a minor impact on our estimate of k. We have also treated the potential as quasistatic. Whereas this is probably a good approximation, it the gigahertz frequency might resonate with long wavelengths off-plane MgO phonons that would definitely change the Ti-tip distance, very important for the exchange modulation mechanism [11,26] and perhaps the Ti-O distance as well.

The g factor observed experimentally for Ti-H/MgO is $g \simeq 1.8$ for magnetic fields pointing almost in plane. From our theory, we expect a larger value, closer to $g_x = 1.97$. There are two possible reasons for this discrepancy. First, the coupling to silver, ignored both in our DFT calculation and in the model, could distort slightly the electronic cloud of Ti-H, which would in turn change D and F and thereby g_x and g_z. Second, and also related to silver, the Kondo coupling to the substrate electrons is expected to renormalize g, in analogy to the Knight shift [49,50]. In the case of an isotropic interaction, the renormalization of the g factor reads, up to first order in the Kondo exchange between the adatom and the substrate electrons, J_s:

$$\delta \Delta_z = -\frac{\Delta_z}{2} g_s \rho J_s, \tag{51}$$

where ρ_s is the density of states of substrate at the Fermi energy and g_s is the g factor of the substrate electrons. The sign of J_s is positive for antiferromagnetic exchange, which is expected in this system, since Kondo effect was observed for Cu/MgO [10]. Therefore, the Kondo interaction could reduce the g factor of Ti-H.

We now summarize the main results of this work:

(1) We have shown that an anisotropic time-dependent modulation of the g tensor induces electronic spin transitions, described by Hamiltonian Eq. (5) and characterized by a Rabi coupling given in Eq. (6).

(2) We have worked out an analytical theory for the anisotropic g factor of the Ti-H $S = 1/2$ adatom on MgO and we have benchmarked it against DFT calculations. Our theory relates g with crystal field parameters D and F, as well as Ti spin orbit coupling λ [Eqs. (15) and (22) and Fig. 4].

(3) We have computed the modulation of the g-tensor anisotropy due to the piezoelectric strain of the Ti-H chemisorbed on an oxygen atom on MgO and we have estimated the resulting Rabi coupling (see Fig. 6). We have found that is much smaller than the one observed experimentally, confirming the dominance of the exchange modulation mechanism [11,26]. However, we have shown that for heavier adatoms with much larger spin orbit coupling λ, this mechanism could be efficient.

(4) We have studied to what extent the crystal field mechanism for EPR-STM, proposed by Baumann *et al.* to

understand the experiments for Fe on MgO [3], could be ascribed to the modulation of the g factor. We find that the dominant contributions to the crystal field mechanism come from the modulation of the zero field splitting parameters.

(5) We have also proposed that a DC voltage can shift the g factor and thereby the Zeeman splitting, and we have computed the effect for the case of Ti-H [see Eq. (50) and Fig. 8]. This shift provides an additional knob to fine-tune the resonance frequency.

(6) We have discussed the impact on the hyperfine coupling of the g-factor anisotropy and its electric modulation [see Eq. (34)].

(7) We have discussed the role of the g-factor anisotropy of Ti-H/MgO to enable the exchange-modulation mechanism for EPR-STM [Eq. (48)]. In the absence of adatom g-factor anisotropy, the exchange-modulation EPR-STM mechanism can only work if the tip moment is not aligned with the applied field [see Eq. (49)].

In this work, we have focused mostly on Ti-H/MgO and Fe/MgO, although most of the ideas can be applied or extended to the case of other atoms. Most notably, the case of Cu/MgO will be the subject of a future publication.

APPENDIX A: CALCULATION OF RABI CONSTANT FOR SPIN MODEL

In this Appendix, we compute the Rabi coupling defined in Eq. (5). We consider the general situation for a $S = 1/2$:

$$\mathcal{H} = \vec{b}_0 \cdot \vec{S} + \vec{b}_1(t) \cdot \vec{S}, \tag{A1}$$

where

$$\vec{b}_0 = |\vec{b}_0|(\sin\theta_0, 0, \cos\theta_0) \tag{A2}$$

and

$$\vec{b}_1(t) = |\vec{b}_1|\cos(2\pi f t)(\sin\theta_1, 0, \cos\theta_1). \tag{A3}$$

We shall give explicit expressions for $\vec{b}_0$ and $\vec{b}_1$ below, where we consider independently the exchange modulation and the g-factor modulation mechanism.

The eigenstates of $H_{=}\mu_B \vec{b}_0 \cdot \vec{S}$ satisfy $H_0|\pm\rangle = \pm\mu_B|\vec{b}_0||\pm\rangle$ and are given by

$$|+\rangle = \cos\frac{\theta_0}{2}|\uparrow\rangle + \sin\frac{\theta_0}{2}|\downarrow\rangle, \tag{A4}$$

$$|-\rangle = \sin\frac{\theta_0}{2}|\uparrow\rangle - \cos\frac{\theta_0}{2}|\downarrow\rangle. \tag{A5}$$

We obtain the matrix element of the spin operators in the basis of eigenstates:

$$\langle+|S_x|-\rangle = \frac{1}{2}\left(\sin^2\frac{\theta_0}{2} - \cos^2\frac{\theta_0}{2}\right) = -\frac{1}{2}\cos\theta_0, \tag{A6}$$

$$\langle+|S_z|-\rangle = \sin\frac{\theta_0}{2}\cos\frac{\theta_0}{2} = \frac{1}{2}\sin\theta_0. \tag{A7}$$

We can now write the general expression

$$\Omega = \frac{|\vec{b}_1|}{2}(-\sin\theta_1\cos\theta_0 + \cos\theta_1\sin\theta_0). \tag{A8}$$

This can be further simplified to

$$\Omega = \frac{|\vec{b}_1|}{2}\sin(\theta_1 - \theta_0) = \frac{1}{2}\frac{\vec{b}_0 \cdot \vec{b}_1}{|\vec{b}_0|}. \tag{A9}$$

1. Expression for Ω for the g-factor modulation

We now apply Eq. (A9) for the case of the g-factor modulation. We now write up

$$\vec{b}_0 = \mu_B(g_x B_x, 0, g_z B_z) \tag{A10}$$

and

$$\vec{b}_1 = \mu_B(\delta g_x B_x, 0, \delta g_z B_z). \tag{A11}$$

Explicitly, we write

$$\sin\theta_0 = \frac{g_x B_x}{\sqrt{(g_x B_x)^2 + (g_z B_z)^2}} \tag{A12}$$

and

$$\cos\theta_0 = \frac{g_z B_z}{\sqrt{(g_x B_x)^2 + (g_z B_z)^2}}. \tag{A13}$$

We thus write

$$\Omega = \frac{\mu_B}{2}(-\delta g_x B_x \cos\theta + \delta g_z B_z \sin\theta). \tag{A14}$$

We now use Eqs. (A12) and (A13) to express B_x and B_y in terms of $\theta, g_x, g_z, B_x, B_z$ and we obtain

$$\Omega = \frac{\mu_B}{2}|\vec{b}_0|\cos\theta_0\sin\theta_0\left(-\frac{\delta g_x}{g_x} + \frac{\delta g_z}{g_z}\right). \tag{A15}$$

Now we use $\cos\theta_0\sin\theta_0 = \frac{1}{2}\sin 2\theta_0$ to obtain

$$\Omega = \frac{\mu_B}{4}|\vec{b}_0|\sin 2\theta_0\left(\frac{\delta g_z}{g_z} - \frac{\delta g_x}{g_x}\right). \tag{A16}$$

We now write the Zeeman splitting

$$\Delta_Z = \mu_B|\vec{b}_0|, \tag{A17}$$

so that we obtain the expression

$$\Omega = \frac{\Delta_Z}{4}\sin 2\theta\left(\frac{\delta g_z}{g_z} - \frac{\delta g_x}{g_x}\right). \tag{A18}$$

2. Expression for Ω for the exchange modulation

We now consider a Hamiltonian for a $S = 1/2$ surface spin where, in addition to the Zeeman interaction, there is a exchange coupling to the magnetic moment of the tip:

$$\mathcal{V}_{exch} = J(z)\vec{n}_T \cdot \vec{S}, \tag{A19}$$

where

$$\vec{n}_T = [\cos(\theta_B + \delta), 0, \sin(\theta_B + \delta)] \tag{A20}$$

and $\vec{B} = B_0(\cos(\theta_B), 0, \sin(\theta_B))$.

We define the spin splitting

$$\Delta_Z^* \equiv \sqrt{(g_x \mu_B B_x + J n_x)^2 + (g_z \mu_B B_z + J n_z)^2} \tag{A21}$$

and we express the angles as

$$\sin\theta_0 = \frac{g_x B_x + J n_x}{\Delta_Z^*} \tag{A22}$$

and

$$\cos\theta_0 = \frac{g_z B_z + J n_z}{\Delta_Z^*}. \tag{A23}$$

For the time-dependent component, we now *ignore* the modulation of the g factors and we only consider the modulation of the exchange that we write up as $\delta J \cos 2\pi f t$. We thus can write

$$\vec{b}_1(t) = \delta J(n_x, 0, n_z). \tag{A24}$$

After some algebra, we obtain

$$\Omega_J = \frac{\delta J}{2\Delta_z^*}(g_x \mu_B . B_x n_z - g_z \mu_B B_z n_x). \tag{A25}$$

Since we are interested in the role of the g-factor anisotropy, we make it explicit and we write

$$g_x = g + \Delta g_x,$$
$$g_z = g + \Delta g_z, \tag{A26}$$

where Δg_x and Δg_z are the static contributions to the g-factor anisotropy. We now define

$$\mathcal{E}_J \equiv \frac{\delta J}{2\Delta_z^*}g\mu_B B \tag{A27}$$

so that the expression for the Rabi reads

$$\Omega_J = \mathcal{E}_J \left(\cos\theta_B \sin(\theta_B + \delta) - \sin\theta_B \cos(\theta_B + \delta)\right)$$
$$+ \mathcal{E}_J \left(\frac{\Delta g_x}{g}\cos\theta_B \sin(\theta_B+\delta) - \frac{\Delta g_z}{g}\sin\theta_B \cos(\theta_B+\delta)\right).$$

We can now write this up as

$$\Omega_J = \mathcal{E}_J \sin\delta$$
$$+ \mathcal{E}_J \left(\frac{\Delta g_x}{g}\cos\theta_B \sin(\theta_B+\delta) - \frac{\Delta g_z}{g}\sin\theta_B \cos(\theta_B+\delta)\right).$$

After some algebra, we obtain

$$\Omega_J = \mathcal{E}_J \sin\delta + \mathcal{E}_J \left(\frac{\Delta g_x}{g} - \frac{\Delta g_z}{g}\right)\cos\theta_B \sin\theta_B \cos\delta$$
$$+ \mathcal{E}_J \left(\frac{\Delta g_x}{g}\cos^2\theta_B + \frac{\Delta g_z}{g}\sin^2\theta_B\right)\sin\delta. \tag{A28}$$

APPENDIX B: ESTIMATION OF SOC FROM NIST DATABASE

From the NIST database [51], we obtain the experimental values for Ti(IV) with an outermost electronic configuration d^1. The lowest energy levels have $L = 2$ and $S = 1/2$, with $J = 3/2$ and $J = 5/2$. Their energy splitting is $\Delta E = 47.3$ meV. We can relate this to the spin orbit coupling using $J = L + S$ and

$$\lambda \vec{L} \cdot \vec{S} = \frac{\lambda}{2}[J(J+1) - L(L+1) - S(S+1)]. \tag{B1}$$

From here, we obtain

$$E(J) = \frac{\lambda}{2}[J(J+1) - L(L+1) - S(S+1)] \tag{B2}$$

and

$$E(J+1) - E(J) = \frac{\lambda}{2}[J + 1(J + 2 - J)] = (J+1)\lambda. \tag{B3}$$

Since $J + 1 = \frac{5}{2}$, we obtain $\lambda_{\text{IV}} = \frac{2}{5}\Delta E_{\text{IV}} = 18.9$ meV. If we consider Ti(III), we have $J + 1 = 3$ and $\Delta E_{\text{III}} = 22.9$ meV. This yields $\lambda_{\text{IV}} = \frac{1}{3}\Delta E_{\text{III}} = 7.63$.

It is apparent that the strength of the atomic spin orbit coupling depends on the charge imbalance in the Ti. One can expect that value of λ for Ti-H on MgO must be in between these two values.

APPENDIX C: RELATION BETWEEN THE $(\ell^+)^4 + (\ell^-)^4$ AND THE $\ell_x^4 + \ell_y^4$ TERMS

In this Appendix, we discuss the connection between these two crystal field operators that we have used for Ti and Fe. The choice is a matter of convenience. After some algebra, the relation between these two operators is

$$\ell_x^4 + \ell_y^4 = \frac{(\ell^+)^4 + (\ell^-)^4}{8} + 24I - \frac{91}{12}\ell_z^2 + \frac{7}{12}\ell_z^4. \tag{C1}$$

Thus, it is apparent that the last two terms can can be reabsorbed as a renormalization of the $D\ell_z^2$ term, plus a shift of the $\ell_z = 0$ level, that plays a very minor role in the discussion for Ti-H/MgO.

[1] Y. Manassen, R. J. Hamers, J. E. Demuth, and A. J. Castellano, Jr., Phys. Rev. Lett. **62**, 2531 (1989).

[2] A. V. Balatsky, M. Nishijima, and Y. Manassen, Adv. Phys. **61**, 117 (2012).

[3] S. Baumann, W. Paul, T. Choi, C. P. Lutz, A. Ardavan, and A. J. Heinrich, Science **350**, 417 (2015).

[4] F. D. Natterer, K. Yang, W. Paul, P. Willke, T. Choi, T. Greber, A. J. Heinrich, and C. P. Lutz, Nature (London) **543**, 226 (2017).

[5] T. Choi, W. Paul, S. Rolf-Pissarczyk, A. J. Macdonald, F. D. Natterer, K. Yang, P. Willke, C. P. Lutz, and A. J. Heinrich, Nat. Nanotech. **12**, 420 (2017).

[6] K. Yang, Y. Bae, W. Paul, F. D. Natterer, P. Willke, J. L. Lado, A. Ferrón, T. Choi, J. Fernández-Rossier, A. J. Heinrich *et al.*, Phys. Rev. Lett. **119**, 227206 (2017).

[7] P. Willke, W. Paul, F. D. Natterer, K. Yang, Y. Bae, T. Choi, J. Fernández-Rossier, A. J. Heinrich, and C. P. Lutz, Sci. Adv. **4**, eaaq1543 (2018).

[8] P. Willke, Y. Bae, K. Yang, J. L. Lado, A. Ferrón, T. Choi, A. Ardavan, J. Fernández-Rossier, A. J. Heinrich, and C. P. Lutz, Science **362**, 336 (2018).

[9] Y. Bae, K. Yang, P. Willke, T. Choi, A. J. Heinrich, and C. P. Lutz, Sci. Adv. **4**, eaau4159 (2018).

[10] K. Yang, P. Willke, Y. Bae, A. Ferrón, J. L. Lado, A. Ardavan, J. Fernández-Rossier, A. J. Heinrich, and C. P. Lutz, Nat. Nanotech. **13**, 1120 (2018).

[11] K. Yang, W. Paul, F. D. Natterer, J. L. Lado, Y. Bae, P. Willke, T. Choi, A. Ferrón, J. Fernández-Rossier, A. J. Heinrich *et al.*, Phys. Rev. Lett. **122**, 227203 (2019).

[12] P. Willke, K. Yang, Y. Bae, A. J. Heinrich, and C. P. Lutz, Nat. Phys. **15**, 1005 (2019).

[13] P. Willke, A. Singha, X. Zhang, T. Esat, C. Lutz, A. J. Heinrich, and T. Choi, Nano Lett. **19**, 8201 (2019).

[14] F. D. Natterer, F. Patthey, T. Bilgeri, P. R. Forrester, N. Weiss, and H. Brune, Rev. Sci. Instrum. **90**, 013706 (2019).

[15] T. Seifert, S. Kovarik, C. Nistor, L. Persichetti, S. Stepanow, and P. Gambardella, arXiv:1908.03379 (unpublished).

[16] S. Thiele, F. Balestro, R. Ballou, S. Klyatskaya, M. Ruben, and W. Wernsdorfer, Science **344**, 1135 (2014).

[17] C. Godfrin, A. Ferhat, R. Ballou, S. Klyatskaya, M. Ruben, W. Wernsdorfer, and F. Balestro, Phys. Rev. Lett. **119**, 187702 (2017).

[18] E. I. Rashba, Sov. Phys. Solid State **2**, 1109 (1960).

[19] Y. Kato, R. Myers, D. Driscoll, A. Gossard, J. Levy, and D. Awschalom, Science **299**, 1201 (2003).

[20] Y. Tokura, W. G. van der Wiel, T. Obata, and S. Tarucha, Phys. Rev. Lett. **96**, 047202 (2006).

[21] M. Pioro-Ladriere, T. Obata, Y. Tokura, Y.-S. Shin, T. Kubo, K. Yoshida, T. Taniyama, and S. Tarucha, Nat. Phys. **4**, 776 (2008).

[22] R. L. Bell, Phys. Rev. Lett. **9**, 52 (1962).

[23] R. E. George, J. P. Edwards, and A. Ardavan, Phys. Rev. Lett. **110**, 027601 (2013).

[24] B. M. Hoffman, J. Phys. Chem. **98**, 11657 (1994).

[25] P. Berggren and J. Fransson, Sci. Rep. **6**, 25584 (2016).

[26] J. L. Lado, A. Ferrón, and J. Fernández-Rossier, Phys. Rev. B **96**, 205420 (2017).

[27] A. M. Shakirov, A. N. Rubtsov, and P. Ribeiro, Phys. Rev. B **99**, 054434 (2019).

[28] J. Reina Galvez, C. Wolf, F. Delgado, and N. Lorente, Phys. Rev. B **100**, 035411 (2019).

[29] Given the C_4 symmetry of the adatom on the oxygen position in MgO, x and y directions are equivalent and we assume $B_y = 0$.

[30] P. Giannozzi, S. Baroni, N. Bonini, M. Calandra, R. Car, C. Cavazzoni, D. Ceresoli, G. L. Chiarotti, M. Cococcioni, I. Dabo *et al.*, J. Phys.: Condens. Matter **21**, 395502 (2009).

[31] J. P. Perdew, K. Burke, and M. Ernzerhof, Phys. Rev. Lett. **80**, 891 (1998).

[32] P. E. Blöchl, Phys. Rev. B **50**, 17953 (1994).

[33] C. J. Pickard and F. Mauri, Phys. Rev. Lett. **88**, 086403 (2002).

[34] S. Baumann, F. Donati, S. Stepanow, S. Rusponi, W. Paul, S. Gangopadhyay, I. G. Rau, G. E. Pacchioni, L. Gragnaniello, M. Pivetta *et al.*, Phys. Rev. Lett. **115**, 237202 (2015).

[35] M. J. Klein, Am. J. Phys. **20**, 65 (1952).

[36] A. Garg, Europhys. Lett. **22**, 205 (1993).

[37] W. Wernsdorfer and R. Sessoli, Science **284**, 133 (1999).

[38] F. Delgado, S. Loth, M. Zielinski, and J. Fernández-Rossier, Europhys. Lett. **109**, 57001 (2015).

[39] R. E. George, W. Witzel, H. Riemann, N. V. Abrosimov, N. Nötzel, M. L. W. Thewalt, and J. J. L. Morton, Phys. Rev. Lett. **105**, 067601 (2010).

[40] M. Shafiei, K. C. Nowack, C. Reichl, W. Wegscheider, and L. M. K. Vandersypen, Phys. Rev. Lett. **110**, 107601 (2013).

[41] E. B. Royce and N. Bloembergen, Phys. Rev. **131**, 1912 (1963).

[42] H. Malissa, W. Jantsch, M. Mühlberger, F. Schäffler, Z. Wilamowski, M. Draxler, and P. Bauer, Appl. Phys. Lett. **85**, 1739 (2004).

[43] J. H. Prechtel, F. Maier, J. Houel, A. V. Kuhlmann, A. Ludwig, A. D. Wieck, D. Loss, and R. J. Warburton, Phys. Rev. B **91**, 165304 (2015).

[44] S. Datta and B. Das, Appl. Phys. Lett. **56**, 665 (1990).

[45] E. Kawakami, P. Scarlino, D. R. Ward, F. Braakman, D. Savage, M. Lagally, M. Friesen, S. N. Coppersmith, M. A. Eriksson, and L. Vandersypen, Nat. Nanotech. **9**, 666 (2014).

[46] A. Laucht, J. T. Muhonen, F. A. Mohiyaddin, R. Kalra, J. P. Dehollain, S. Freer, F. E. Hudson, M. Veldhorst, R. Rahman, G. Klimeck *et al.*, Sci. Adv. **1**, e1500022 (2015).

[47] A. Ferrón, F. Delgado, and J. Fernández-Rossier, New J. Phys. **17**, 033020 (2015).

[48] A. Ferrón, J. L. Lado, and J. Fernández-Rossier, Phys. Rev. B **92**, 174407 (2015).

[49] D. C. Langreth and J. W. Wilkins, Phys. Rev. B **6**, 3189 (1972).

[50] F. Delgado, C. Hirjibehedin, and J. Fernández-Rossier, Surf. Sci. **630**, 337 (2014).

[51] D. E. Kelleher, W. C. Martin, W. L. Wiese, J. Sugar, J. R. Fuhr, K. Olsen, A. Musgrove, P. J. Mohr, J. Reader, and G. Dalton, Phys. Scr. **T83**, 158 (1999).